*J. Plasma Physics* (1999), *vol.* 62, *part* 4, *pp.* 425–439. Printed in the United Kingdom 


# Beam stability in strongly magnetized pair plasmas. Part 1

G. W. ROWE and E. T. ROWE

Special Research Centre for Theoretical Astrophysics, School of Physics, Sydney University, NSW 2006, Australia

(Received 1 December 1998 and in revised form 5 July 1999)

**Abstract.** We present a detailed *ab initio* calculation of wave modes in a strongly magnetized pair-plasma slab (which we shall refer to as a beam) embedded in a pair plasma of different number density. We consider a planar geometry and treat the case of small beam thickness, for which approximate analytical results can be obtained and compared with numerical calculations. We briefly compare our results with those found by others in the case of cylindrical geometry as applied in the context of radio pulsars.

## 1. Introduction

Curvature emission by charged particles moving along a strong curved magnetic field is a mechanism that is often invoked to explain radio emission from pulsars. There is, however, no generally accepted theory of pulsar radio emission that accounts for the coherence required to explain the observations while appealing to the curvature of magnetic field lines alone. A recently suggested mechanism for pulsar radio emission includes boundary effects in the treatment of the emission region of the magnetosphere (Asséo et al. 1983 – hereinafter referred to as APS83; Asséo 1995 – hereinafter referred to as A95), with the introduction of sharp boundaries claimed to be an essential ingredient in allowing instabilities to arise. In this scenario, a beam of pair plasma streams along curved magnetic field lines, bounded on either side by plasmas with different particle number densities. The system is modelled locally in cylindrical geometry, with the exterior radius of the beam being equated to the local radius of curvature of the magnetic field lines and assuming infinite magnetic field strength. Three types of instabilities are thought to be possible: a radiative instability, identical to that considered by Goldreich and Keeley (1971) and Buschauer and Benford (1978, 1979), a two-stream instability, and a new so-called 'finite beam instability'. APS83 and A95 suggest that the finite beam instability is a prime candidate for radio emission close to the neutron star surface, while the radiative instability may be one possibility for radio emission further out in the magnetosphere. The invocation of at least two emission mechanisms is consistent with the separation of pulsar emission into core and conal components, as suggested by Rankin (1992).

This is the first of two papers in which we consider a pair plasma beam streaming between bounding pair plasmas of different number densities in planar geometry, rather than cylindrical. A detailed analysis of the planar-geometry case is useful

for a number of reasons. An early treatment of the strong (essentially infinite)-magnetic-field case appeared in Schmidt (1979) for a cold-plasma slab at rest and immersed in a vacuum, for which a dispersion relation was derived; but solutions in the form of our 'thin-beam' results were overlooked. These solutions are important, since they are related to the cylindrical-geometry results of APS83 and A95, which lead to their version of the radiative instability. In the case of a slab flowing relative to an external medium other than vacuum, these solutions can also be shown, as we do here, to give rise to instability in planar geometry. The planar-geometry case for a beam bounded by vacuum was considered by Asséo et al. (1980), but in that work the thin-beam solutions were not considered, and the dielectric constant for the beam contained both slow and fast components (here we consider only one component). The instabilities found were not due to the presence of sharp boundaries but rather the presence of the two components. The results that we present here allow a detailed understanding of the planar-geometry case, for a beam with arbitrary flow velocity bounded by vacuum or by a pair plasma.

A second reason for the calculations is to highlight the fact that, in dealing with bounded systems, one must take care in identifying instability, since the presence of boundaries allows the input of wave energy from the external media. One must identify the velocity of energy propagation in these media in order to determine whether or not temporal growth of wave modes is accompanied by a net outflow of energy from the beam (instability) or a net inflow of energy (no instability). In the planar case, identification of the velocity of energy propagation is relatively straightforward (although not trivial, since it is not always equivalent to the usual group velocity), and we give forms for it that we use to interpret the stability or otherwise of the wave modes. In particular, these forms reproduce the expected result that, for a given plasma, the introduction of boundaries with vacuum (making the plasma a slab) does not alter the stability properties.

The thin-beam results alluded to above apply when the thickness of the beam is sufficiently small. As mentioned above, a thin-beam case in cylindrical geometry, leading to a form of radiative instability, was described by APS83 and A95 and is related to our results in planar geometry. One expects that if the beam is sufficiently thin, and the radius of curvature of the beam is sufficiently large, then any difference should be accounted for by the choice of global geometry (or equivalently boundary conditions applied away from the beam interfaces), since curvature effects become higher-order corrections and the wave inside the beam does not resolve the curvature. We hope to use the results presented here to consider this in more detail elsewhere.

In Sec. 2, we summarize the properties of waves propagating in a pair plasma streaming along a straight superstrong magnetic field (effectively infinite). These properties are then used in Sec. 3 to derive the dispersion equation for waves propagating in a beam bounded by plasma, assuming planar geometry. Section 4 details the thin-beam solutions for waves in the bounded beam system with frequencies around the beam resonance frequency. For bounding plasmas with non-zero plasma frequency, the natures of the thin-beam solutions depend on the wavenumber parallel to the beam. For 'short-wavelength' waves the beam is stable but for 'long-wavelength' waves instability is possible. In Sec. 5, we summarize the results and briefly compare them with those of APS83 and A95. SI units are used throughout.

## 2. Wave modes in a homogeneous pair plasma

Writing the electric field $\mathbf{E}(t, \mathbf{x})$ in terms of its Fourier transform

$$\mathbf{E}(t, \mathbf{x}) = \int \frac{d\omega\, d\mathbf{k}}{(2\pi)^4}\, e^{i(\mathbf{k}\cdot\mathbf{x}-\omega t)}\mathbf{E}(\omega, \mathbf{k}), \tag{2.1}$$

and similarly for other field quantities, the linearized Maxwell equations reduce to the homogeneous wave equation

$$[n^2(\boldsymbol{\kappa}\boldsymbol{\kappa} - \boldsymbol{\delta}) + \mathbf{K}(\omega, \mathbf{k})]\mathbf{E}(\omega, \mathbf{k}) = 0, \tag{2.2}$$

where the refractive index $n = ck/\omega$, the normalized wavevector $\boldsymbol{\kappa} = \mathbf{k}/k$, $k = |\mathbf{k}|$ and $\mathbf{K}(\omega, \mathbf{k})$ is the dielectric tensor.

Consider a homogeneous electron–positron pair plasma immersed in a strong magnetic field directed along the $\hat{\mathbf{z}}$ axis. Assuming that all electrons and positrons flow along the magnetic field with speed $U$, the dielectric tensor takes the form $\mathbf{K}(\omega, \mathbf{k}) = \boldsymbol{\delta} + (W - 1)\hat{\mathbf{z}}\hat{\mathbf{z}}$, with $\boldsymbol{\delta}$ the unit tensor and

$$W = 1 - \frac{\omega_p^2}{\gamma_p^3(\omega - k_\parallel U)^2}. \tag{2.3}$$

Here $\omega_p$ is the total plasma frequency, $\gamma_p$ is the Lorentz factor of the plasma, and we use the notations $k_\parallel$ and $k_z$ interchangeably. The assumption of a strong magnetic field requires that the cyclotron frequency $\boldsymbol{\Omega}_e \gg \omega_p, kU, \omega$ and is of relevance in an application to pulsars. As the dielectric tensor is Hermitian, there is neither absorption of wave energy nor any kinetic instability (negative absorption). Another important feature is the wave–particle resonance at the beam resonance frequency $\omega_R = k_\parallel U$.

One obtains non-trivial solutions for $\mathbf{E}(\omega, \mathbf{k})$ when the determinant $\Lambda(\omega, \mathbf{k})$ of the matrix in (2.2) vanishes:

$$\Lambda(\omega, \mathbf{k}) = (1 - n^2)[W(1 - n^2\kappa_\parallel^2) - n^2\kappa_\perp^2] = 0, \tag{2.4}$$

where $\kappa_\perp^2 = \kappa_x^2 + \kappa_y^2$. It can be shown that for these solutions $\omega$ is real for real $\mathbf{k}$, indicating that there are no reactive instabilities. One solution is $n^2 = 1$, corresponding to vacuum-like waves that are not coupled to plasma oscillations, and we do not consider this mode further here. For the purposes of this paper, it is expedient to write down the second solution for $k_x^2$ rather than $n^2$:

$$k_{x2}^2 = \frac{\omega^2}{c^2}W\left(1 - \frac{c^2k_z^2}{\omega^2}\right) - k_y^2. \tag{2.5}$$

Confining our attention to $k_y = 0$, the second mode is conveniently written in the form

$$\mathbf{E}(\omega, \mathbf{k}) = \frac{c^2}{\omega W}[B^+(\omega, \mathbf{k}_s)2\pi\delta(k_x - k_{x2}) + B^-(\omega, \mathbf{k}_s)2\pi\delta(k_x + k_{x2})](Wk_z, 0, -k_x), \tag{2.6}$$

$$\mathbf{B}(\omega, \mathbf{k}) = [B^+(\omega, \mathbf{k}_s)2\pi\delta(k_x - k_{x2}) + B^-(\omega, \mathbf{k}_s)2\pi\delta(k_x + k_{x2})]\hat{\mathbf{y}}, \tag{2.7}$$

where we account for the two possible solutions $k_x = \pm k_{x2}$, where $k_{x2}$ is defined to be either of the two roots of (2.5). This mode is partly longitudinal and partly transverse, and is associated with both plasma-charge and current-density fluctuations.

https://doi.org/10.1017/S002237789900793X Published online by Cambridge University Press

## 3. Beam geometry and dispersion equation

We consider a beam (or slab) of electrons and positrons all moving along a strong ambient magnetic field directed along the $\hat{\mathbf{z}}$ axis, as for the homogeneous plasma of Sec. 2, and bounded by similar pair plasmas. We assume that the beam, of thickness $a$, is situated between the planes $x = x_0$ and $x = x_0 + a$ and is of infinite extent in the $y$ and $z$ directions. The dielectric tensors for each of the three plasmas are of the form given in Sec. 2, and $W$ is denoted by $W_l$, $W_r$ and $W_b$ for the plasma on the left of the beam, on the right of the beam and in the beam respectively.

In order to derive the dispersion equation for waves in the beam system, we must apply the appropriate boundary conditions at both interfaces of the beam. As the three plasmas are cold and the ambient magnetic field is uniform over all space, we are free to assume that there are no surface currents on the two interfaces. The relevant boundary conditions in that case are that the tangential (to the interfaces) components of both the electric and magnetic fields are continuous across the interfaces. Assuming that in the bounding plasmas $B^-(\omega, \mathbf{k}_s) = 0$, the boundary conditions applied to wave fields of the form (2.1) with (2.6) and (2.7) can be written as a matrix equation

$$\begin{pmatrix} e^{ik_x^l x_0} & -e^{ik_x^b x_0} & -e^{-ik_x^b x_0} & 0 \\ 0 & e^{ik_x^b (x_0+a)} & e^{-ik_x^b (x_0+a)} & -e^{ik_x^r (x_0+a)} \\ -\dfrac{k_x^l}{W_l} e^{ik_x^l x_0} & \dfrac{k_x^b}{W_b} e^{ik_x^b x_0} & -\dfrac{k_x^b}{W_b} e^{-ik_x^b x_0} & 0 \\ 0 & -\dfrac{k_x^b}{W_b} e^{ik_x^b (x_0+a)} & \dfrac{k_x^b}{W_b} e^{-ik_x^b (x_0+a)} & \dfrac{k_x^r}{W_r} e^{ik_x^r (x_0+a)} \end{pmatrix} \begin{pmatrix} B_l^+ \\ B_b^+ \\ B_b^- \\ B_r^+ \end{pmatrix} = 0. \tag{3.1}$$

The superscripts and subscripts $l$, $r$ and $b$ refer to the three plasmas as before, and we have dropped the subscript 2 on $k_{x2}$ for convenience. In choosing $B^-(\omega, \mathbf{k}_s) = 0$, we restrict our discussion to waves with one sign of $k_x$ in each of the bounding media. This precludes wave reflections at the interfaces, and is consistent with looking for normal modes of the system. The dispersion equation obtained is

$$\left[\left(\frac{k_x^b}{W_b}\right)^2 - \frac{k_x^l}{W_l}\frac{k_x^r}{W_r}\right] \sin(k_x^b a) + i\frac{k_x^b}{W_b}\left(\frac{k_x^r}{W_r} - \frac{k_x^l}{W_l}\right) \cos(k_x^b a) = 0, \tag{3.2}$$

and is to be solved for the wave frequency $\omega$ in terms of the surface wavenumber $k_\parallel$.

The dispersion equation simplifies when the two bounding plasmas are identical ($W_l \equiv W_r$). Then $(k_x^l)^2 = (k_x^r)^2$ and, choosing $k_x^l = -k_x^r$ (a natural choice given the reflection symmetry of the problem), (3.2) requires that either $k_x^r / W_r = 0$ or

$$\left(\frac{1}{W_r} + \frac{1}{W_b}\right) k_x^r \sin(k_x^b a) + 2i\frac{k_x^b}{W_b} \cos(k_x^b a) = 0, \tag{3.3}$$

where, in the rest frame of the bounding plasma,

$$W_l \equiv W_r = 1 - \frac{\omega_{pr}^2}{\omega^2}, \tag{3.4a}$$

$$W_b = 1 - \frac{\omega_p^2}{\gamma_p^3 (\omega - k_\parallel U)^2}. \tag{3.4b}$$

Here $\omega_{pr}$ is the rest-frame total plasma frequency of the bounding plasma, and, for convenience, we do not label the beam total plasma frequency or Lorentz factor

https://doi.org/10.1017/S002237789900793X Published online by Cambridge University Press

with a subscript $b$. We note that we could also have chosen $k_x^l = k_x^r$ in the above, but that choice does not lead to solutions of interest here. The equation $k_x^r/W_r = 0$ leads to formal solutions $\omega = 0$ (a static wave with $k_x^r = \pm\infty$, implying a perpendicular wavelength of zero in the external media) and $\omega = \pm ck_\parallel$ (a wave propagating with phase speed $c$ along the beam), which are also not of interest here. In order to solve (3.3) in general, a numerical approach is required; however, one may prove that, given a complex solution $\delta\omega$ with $k_x^r = k_x$, the complex conjugate $\delta\omega^*$ is also a solution with $k_x^r = -k_x^*$.

If the beam thickness $a$ is sufficiently small, the dispersion equation (3.3) has approximate analytical solutions around the beam resonance frequency $\omega_R = k_\parallel U$ of the form $\omega \approx \omega_R + \delta\omega + O[(\delta\omega)^2]$, where $|\delta\omega| \ll |\omega_R|$. The reality condition implies that we need only consider $\omega_R > 0$, and, without loss of generality, we thus assume $U > 0$ and $k_\parallel > 0$ throughout the remainder of the paper. Two categories of solution exist: solutions with $\delta\omega = O(a^{1/2}) \gg a$ and $|k_x^b a| \ll 1$, which will be referred to as thin-beam solutions, and solutions with $\delta\omega = O(a)$ and $|k_x^b a| \geqslant 1$, which will be referred to as thick-beam solutions. Thick-beam solutions are discussed in Part 2 (Rowe and Rowe 1999), together with an alternative thin-beam expansion valid for highly relativistic beams.

## 4. Thin-beam solutions: small-$a$ approximation

Writing $\omega = \omega_R + \delta\omega + O[(\delta\omega)^2]$ and assuming $|\omega_R| \not\approx \omega_{pr}$, one has, from (3.4),

$$W_l = W_r = \left(1 - \frac{\omega_{pr}^2}{\omega_R^2}\right) + O(\delta\omega), \tag{4.1a}$$

$$W_b = -\frac{\omega_p^2}{\gamma_p^3(\delta\omega)^2}[1 + O(\delta\omega)], \tag{4.1b}$$

and, from (2.5),

$$k_x^r = k_{xR}^r\left(1 + \frac{1}{k_{xR}^r}\frac{\delta\omega}{v_{gx}^r}\right) + O(\delta\omega)^2, \tag{4.2a}$$

$$k_x^b = \pm\frac{\omega_p|k_\parallel|}{\gamma_p^{5/2}(\delta\omega)}\left[1 + O(\delta\omega)\right], \tag{4.2b}$$

where

$$(k_{xR}^r)^2 = -\frac{k_\parallel^2}{\gamma_p^2}\left(1 - \frac{\omega_{pr}^2}{\omega_R^2}\right), \tag{4.3}$$

is the square of $k_x^r$ (as given by (2.5)) evaluated at the beam resonance frequency $\omega_R$, and

$$\begin{aligned} v_{gx}^r &= \left.\frac{\partial\omega_2(\mathbf{k})}{\partial k_x}\right|_{\omega_R} = \left.\frac{1}{\partial k_{x2}(\omega, \mathbf{k}_s)/\partial\omega}\right|_{\omega_R} \\ &= \frac{c^2 k_{xR}^r}{\omega_R}\left[1 - \frac{\omega_{pr}^2}{\omega_R^2}\frac{\gamma_p^2}{(\gamma_p^2 - 1)}\right]^{-1}, \end{aligned} \tag{4.4}$$

is the $x$ component of the group velocity $\mathbf{v}_g^r$ of the wave mode in the bounding plasma on the right of the beam, evaluated at $\omega = \omega_R$ (i.e. to lowest order in $\delta\omega$).

https://doi.org/10.1017/S002237789900793X Published online by Cambridge University Press

Note that $\omega_2(\mathbf{k})$ is the frequency that one obtains by solving (2.5) for $\omega$ in terms of $\mathbf{k}$.

Retaining lowest orders only in each contribution to (3.3) and assuming that $a$ is small such that $O(|k_x^b a|) < 1$ (thin-beam assumption), we expand the sine and cosine terms and obtain

$$k_{xR}^r = -\frac{2iW_r}{aW_b}, \tag{4.5}$$

with $W_r$ and $W_b$ as in (4.1). Squaring both sides and using (4.3) leads to

$$(\delta\omega)^4 = \frac{\omega_p^4}{\gamma_p^8(1-\omega_{pr}^2/\omega_R^2)}\left(\frac{k_\parallel a}{2}\right)^2, \tag{4.6}$$

and there are four possible solutions for $\delta\omega$, the natures of which depend upon the sign of $1-\omega_{pr}^2/\omega_R^2$ as discussed below.

### *4.1. Short-wavelength waves*

For short wavelengths satisfying

$$|k_\parallel| > \frac{\omega_{pr}\gamma_p}{c(\gamma_p^2-1)^{1/2}}, \tag{4.7}$$

one has $|\omega_R| > \omega_{pr}$, and (4.6) then has two real solutions $\delta\omega = \pm|\delta\omega|$, which we label $A$ and $B$ respectively, and two imaginary solutions $\delta\omega = \pm|\delta\omega|i$, which we label $C^+$ and $C^-$ respectively, where

$$|\delta\omega| = \frac{\omega_p}{\gamma_p^2|1-\omega_{pr}^2/\omega_R^2|^{1/4}}\left(\frac{|k_\parallel|a}{2}\right)^{1/2}. \tag{4.8}$$

The real solutions ($A$ and $B$) represent waves that are neither temporally growing nor decaying, and in that case $\delta\omega$ is simply a frequency shift. For these waves, evaluation of the right-hand side of (4.5) determines that $k_{xR}^r = |k_{xR}^r|i$, where $|k_{xR}^r|$ can be obtained from (4.3). One finds that, to $O(a^{1/2})$,

$$k_x^r = |k_{xR}^r|i\left(1 \mp \frac{|\delta\omega|}{|k_{xR}^r|^2}\frac{k_{xR}^r}{v_{gx}^r}\right), \tag{4.9}$$

with $k_{xR}^r/v_{gx}^r$ given by (4.4). Thus $k_x^r$ is positive imaginary (since the second term is a small correction) and the waves are bound to the beam, exponentially decaying in amplitude away from the beam in both the positive and negative $x$ directions. There is no real correction to $k_x^r$, and thus no propagation of energy into or out of the beam. Using (4.2b), we can write $k_x^b \approx |k_x^b|$, where

$$|k_x^b| = \left|1-\frac{\omega_{pr}^2}{\omega_R^2}\right|^{1/4}\left(\frac{2|k_\parallel|}{a\gamma_p}\right)^{1/2}, \tag{4.10}$$

and hence the waves are freely propagating inside the beam. The wavelength of waves in the beam is $O(a^{1/2})$, which is greater than the order of the beam thickness (for small $a$), and it is in this sense that the beam is thin.

The imaginary solutions $\delta\omega = \pm|\delta\omega|i$ ($C^+$ and $C^-$) represent waves that are temporally growing and decaying respectively, with growth/decay rate $|\delta\omega|$. For these waves, evaluation of the right-hand side of (4.5) implies that $k_{xR}^r = -|k_{xR}^r|i$,

https://doi.org/10.1017/S002237789900793X Published online by Cambridge University Press

and hence, to $O(a^{1/2})$,

$$k_x^r = -|k_{xR}^r| i \left(1 \mp \frac{|\delta\omega|}{|k_{xR}^r|^2} \frac{k_{xR}^r}{v_{gx}^r} i\right), \tag{4.11}$$

for these solutions. In contrast to modes $A$ and $B$, these waves are not bound to the beam, but rather grow exponentially in amplitude away from the beam, as indicated by the fact that the imaginary part of $k_x^r$ is negative. This spatial growth, along with the temporal growth or decay of the waves, is associated with a real correction to $k_x^r$, indicating that there is a propagation of energy either into or out of the beam. As $k_{xR}^r$ is imaginary, it is clear that the $x$ component of the group velocity $v_{gx}^r$ will also be imaginary, and thus $v_{gx}^r$ cannot correspond to the speed at which energy propagates perpendicular to the beam. The correct identification of the speed of energy propagation perpendicular to the beam in this case is (see the Appendix)

$$\tilde{v}_{gx}^r = \frac{\mathrm{Im}[\delta\omega]}{\mathrm{Im}[k_x^r]} = \mp \frac{|\delta\omega|}{|k_{xR}^r|}, \tag{4.12}$$

where the tilde is used to avoid confusion with $v_{gx}^r$. Hence, the temporally growing waves are associated with an influx of wave energy into the beam from the bounding plasmas, whilst the temporally decaying waves are associated with radiation of energy away from the beam and into the bounding plasmas.

In the case of radiating modes (such as mode $C^-$), spatial growth is a necessary requirement of the solutions. This was discussed to some extent in Rowe (1993) in relation to the kinetic Alfvén mode, by Cally (1986) and by Schmidt (1979). In the case of mode $C^+$, energy is fed into the beam via the inverse of this radiation process, and the temporal growth is not due to an instability. This solution is not a normal mode of the system, but indicates that, under the right conditions, it may be possible for an external source to supply energy to the beam.

For $|k_\parallel| > \omega_{pr}\gamma_p^2/(\gamma_p^2 - 1)c$, the phase velocity $\omega_R/\mathrm{Re}[k_x^r]$ and $\tilde{v}_{gx}^r$ have the same sign, and the waves are referred to as forward-propagating; that is, the waves and the wave energy propagate in the same direction. Conversely, for $|k_\parallel| < \omega_{pr}\gamma_p^2/(\gamma_p^2 - 1)c$, the phase velocity and $\tilde{v}_{gx}^r$ have opposite signs, and we refer to the waves as backward-propagating. Inside the beam, the waves are restricted to the edges of the beam, given that $k_x^b \approx |k_x^b| i$ with (4.10).

### *4.2. Long-wavelength waves*

For long wavelengths satisfying

$$|k_\parallel| < \frac{\omega_{pr}\gamma_p}{c(\gamma_p^2 - 1)^{1/2}}, \tag{4.13}$$

one has $|\omega_R| < \omega_{pr}$, and (4.6) has two pairs of complex-conjugate solutions, which may be written in the forms

$$\delta\omega = \frac{1 \pm i}{\sqrt{2}} |\delta\omega|, \qquad \delta\omega = -\frac{1 \pm i}{\sqrt{2}} |\delta\omega|, \tag{4.14a,b}$$

with $|\delta\omega|$ as given by (4.8). We label the first pair of modes $C^+$ and $C^-$ respectively, since these solutions are related to the short-wavelength modes labelled $C^+$ and $C^-$, and we label the second pair $B^-$ and $B^+$ respectively, since they are related to the short-wavelength $B$ mode, as shown in Fig. 1. In this approximation, there is no long-wavelength equivalent of mode $A$.

https://doi.org/10.1017/S002237789900793X Published online by Cambridge University Press

Modes $C^+$ and $C^-$ correspond to a temporally growing and a temporally decaying wave mode, both of which are frequency-shifted upwards from the beam resonance frequency $\omega_R$. For these waves, evaluation of (4.5) implies that $k^r_{xR} = \pm|k^r_{xR}|$, and then

$$k^r_x \approx \pm|k^r_{xR}|\left(1 + \frac{|\delta\omega|}{|k^r_{xR}|^2}\frac{k^r_{xR}}{v^r_{gx}}\frac{1 \pm i}{\sqrt{2}}\right), \tag{4.15}$$

indicating that, to $O(a^{1/2})$, the waves grow exponentially away from the beam. The real part of $k^r_x$ implies that there is a flow of energy perpendicular to the beam, and, since $k^r_{xR}$ is real, the speed of energy flow in the $x$ direction (to lowest order in $a$) is in this case given by the $x$ component of the group velocity

$$\tilde{v}^r_{gx} \equiv v^r_{gx} = \mp\frac{|\omega^2_{pr}/\omega^2_R - 1|^{1/2}}{(\gamma^2_p - 1)^{1/2}}\left[\frac{\omega^2_{pr}}{\omega^2_R}\frac{\gamma^2_p}{(\gamma^2_p - 1)} - 1\right]^{-1} c, \tag{4.16}$$

which satisfies $|v^r_{gx}| \leqslant c$. For mode $C^-$ there is a flow of energy out of the beam and into the bounding plasma, whilst for mode $C^+$ there is a flow of energy into the beam from the bounding plasma (the sign of $v^r_{gx}$ is opposite that of $\mathrm{Im}[\delta\omega]$). As in the short-wavelength case, mode $C^+$ does not imply an instability nor does mode $C^-$ imply absorption, but rather a source/sink of wave energy that is external to the beam system.

The solutions $B^-$ and $B^+$ correspond to a temporally decaying and a temporally growing wave mode respectively, both of which are frequency-shifted downwards from the beam resonance frequency. Again one finds $k^r_{xR} = \pm|k^r_{xR}|$, and in this case

$$k^r_x \approx \pm|k^r_{xR}|\left(1 - \frac{|\delta\omega|}{|k^r_{xR}|^2}\frac{k^r_{xR}}{v^r_{gx}}\frac{1 \pm i}{\sqrt{2}}\right), \tag{4.17}$$

so the waves decay exponentially into the bounding plasmas and are therefore bound to the beam, to first order. The real part of $k^r_x$ implies an energy flow perpendicular to the beam, and the speed of this flow in the $x$ direction is given by (4.16). The modes $B^-$ and $B^+$ are fundamentally different from the modes $C^+$ and $C^-$, since the temporally decaying mode $B^-$ is associated with an energy flow into the beam, and the temporally growing mode $B^+$ is associated with an outflow of energy. The temporal growth of $B^+$ can be attributed to a reactive instability (or particle bunching), and can be explained in terms of negative (or potential) energy of the forced particle motions in the wave. As the wave amplitude increases, the particle energy becomes increasingly negative, while the bunching of particles enhances the electromagnetic field of the wave, and the electromagnetic energy increases. The total wave energy (electromagnetic plus particle) is negative, and becomes increasingly negative as the wave amplitude grows, corresponding to a flow of electromagnetic energy (positive by definition) out of the beam. The temporal decay of the $B^-$ mode can be attributed to the inverse of this process. A reactive instability of this type is only possible for modes with $\mathrm{Re}[\delta\omega] < 0$, which is a prerequisite for negative particle energy in the beam plasma.

### *4.3. Transition between long and short wavelengths*

In deriving the long- and short-wavelength results, it was assumed that $|\omega_R| \not\approx \omega_{pr}$, and the approximations obtained are not applicable at the transition point between these two types of solution, as indicated by the singularity at $|\omega_R| = \omega_{pr}$. The

https://doi.org/10.1017/S002237789900793X Published online by Cambridge University Press

transition point can be treated by assuming that $|\omega_R| = \omega_{pr}(1+\epsilon)$, or equivalently

$$|k_\parallel| = \frac{\omega_{pr}(1+\epsilon)\gamma_p}{c(\gamma_p^2-1)^{1/2}}, \tag{4.18}$$

where $\epsilon$ is a small parameter.

We may seek a solution of the form $\omega = \omega_0 + \omega_1\epsilon + \ldots$ near the singularity, and the dispersion equation then leads to a transcendental equation for $\omega_0$. In this section, we have assumed that $a$ is small enough so that an expansion in $a$ is valid. We may thus approximate $\omega_0$ by setting $\epsilon = 0$ in (4.18), writing $\omega_0 = \omega_R + \delta\omega$, and, following the procedure we used before, replacing the approximations given in (4.1a) and (4.2a) for $W_r$ and $k_x^r$ by

$$W_l = W_r = 2\frac{\delta\omega}{\omega_R} + O(\delta\omega)^2, \tag{4.19a}$$

$$(k_x^r)^2 = -2\frac{k_\parallel^2}{\gamma_p^2}\frac{\delta\omega}{\omega_R} + O(\delta\omega)^2. \tag{4.19b}$$

Using these approximations, (3.3) reduces to an equation of the same form as (4.5),

$$k_x^r = -\frac{2iW_r}{aW_b}, \tag{4.20}$$

except that in this case $k_x^r$ on the left-hand side is given by the square root of (4.19b). Solutions are found that satisfy $\delta\omega = O(a^{2/5})$ and can be written in the form $\delta\omega = |\delta\omega_s|e^{2ni\pi/5}$, for $n = 0, 1, 2, 3, 4$, where

$$|\delta\omega_s| = \left[\frac{\omega_{pr}^3\omega_p^4a^2}{8\gamma_p^6(\gamma_p^2-1)c^2}\right]^{1/5}. \tag{4.21}$$

Of the five solutions, one is neither temporally growing nor decaying ($n = 0$), and there are two complex-conjugate pairs ($n = 1, 4$) and ($n = 3, 2$), which correspond to temporally growing and decaying waves. For the complex-conjugate solutions, $n$ is the number of the quadrant in the complex plane in which the particular solution appears. The solutions can be written in the explicit form

$$\delta\omega = |\delta\omega_s|, \tag{4.22}$$

$$\delta\omega = |\delta\omega_s|\left(\sin\frac{\pi}{10} \pm i\cos\frac{\pi}{10}\right), \tag{4.23}$$

$$\delta\omega = -|\delta\omega_s|\left(\cos\frac{\pi}{5} \pm i\sin\frac{\pi}{5}\right). \tag{4.24}$$

The wavenumber $k_x^r$ corresponding to these solutions is $k_x^r = |k_{xs}^r|e^{(5+12n)i\pi/10}$, with

$$|k_{xs}^r| = \left[\frac{2\omega_p^2\omega_{pr}^4a}{\gamma_p^3(\gamma_p^2-1)^3c^6}\right]^{1/5}, \tag{4.25}$$

or, explicitly,

$$k_x^r = |k_{xs}^r|i, \tag{4.26}$$

$$k_x^r = \pm|k_{xs}^r|\left(\sin\frac{\pi}{5} \mp i\cos\frac{\pi}{5}\right), \tag{4.27}$$

https://doi.org/10.1017/S002237789900793X Published online by Cambridge University Press

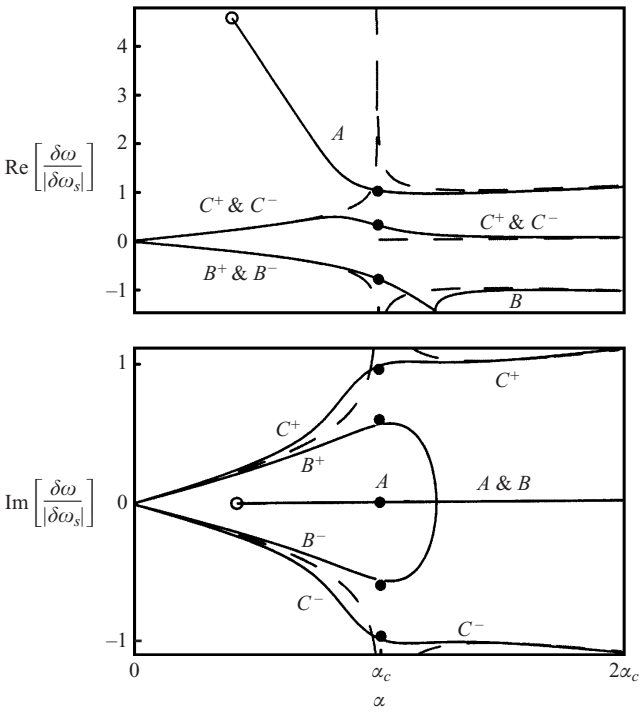


**Figure 1.** Real and imaginary parts of $\delta\omega/|\delta\omega_s|$ for all modes as functions of $\alpha = ck_\parallel/\omega_p$ with $\gamma_p = 1.1$, $\omega_{pr}/\omega_p = 1$ and $a\omega_p/c = 0.01$. The small-$a$ approximation is shown (broken curves) together with numerically calculated results (solid curves). Short-wavelength modes appear to the right of $\alpha_c = c\omega_{pr}/U\omega_p$ and long-wavelength modes to the left, and the filled circles are the transition-point approximations while the open circle indicates the cutoff for mode $A$.

$$k_x^r = \pm|k_{xs}^r|\left(\cos\frac{\pi}{10} \pm i\sin\frac{\pi}{10}\right), \tag{4.28}$$

respectively. To lowest order in $a$, we find that $\omega_1$ is finite and independent of the sign of $\epsilon$, indicating that there is no actual singularity at $|\omega_R| = \omega_{pr}$ and that the dispersion relations are continuous and smooth through that point. The singularity in the approximations for the short- and long-wavelength cases is due to the breakdown of those approximations near $|\omega_R| = \omega_{pr}$ at which point the $a$ dependence of $\delta\omega$ changes from $a^{1/2}$ to $a^{2/5}$.

Our approximate solutions are shown in Fig. 1, together with those obtained by solving the dispersion equation (3.3) numerically, using a secant method with the approximations as initial estimates of the roots. The numerical results verify that the approximations are good for small $a$ and that all the dispersion relations are continuous through the transition point. The approximate solutions for $\delta\omega$ at the transition point may be related to those in the short- and long-wavelength regimes; specifically, (4.24) is identified with $B^-$ and $B^+$, and (4.23) with $C^+$ and $C^-$. After passing through the transition point to the short-wavelength side, modes $B^-$ and $B^+$ coalesce and become negative real (mode $B$), while modes $C^+$ and $C^-$ remain a conjugate pair. The transition-point solution (4.22) is identified with the short-wavelength approximation to mode $A$, which has no long-wavelength counterpart, although mode $A$ can extend into the long-wavelength regime as shown in Fig. 1.

https://doi.org/10.1017/S002237789900793X Published online by Cambridge University Press

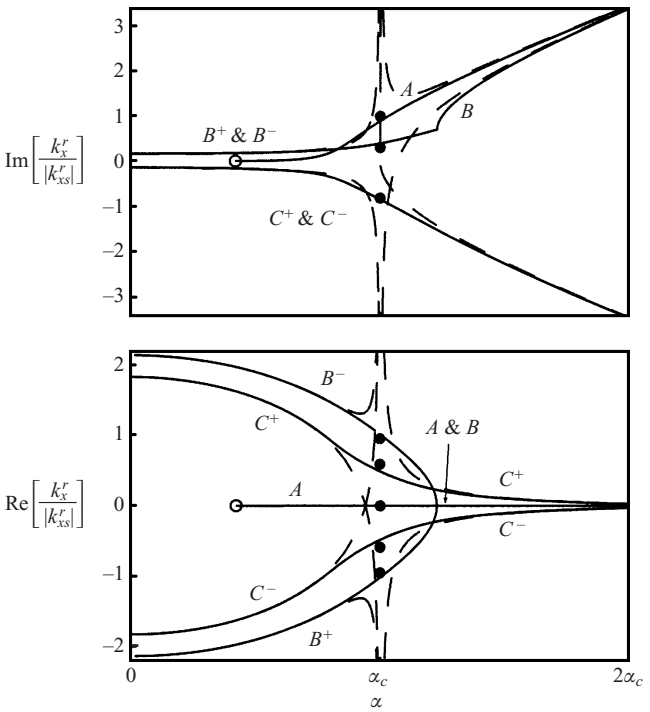


**Figure 2.** Imaginary and real parts of $k_x^r/|k_{xs}^r|$ for all modes as functions of $\alpha = ck_\parallel/\omega_p$ with the same parameter values as for Fig. 1. The broken curves are small-$a$ approximations, the solid curves are numerically calculated results, and the filled circles are the transition-point approximations. The open circle indicates the cutoff for mode $A$.

The behaviour of the real modes ($A$ and $B$) may be further understood by considering the form of $k_x$ given by (2.5) and shown in Fig. 2. For $k_x^2 < 0$ in the external media these modes are bound to the beam, while for $k_x^2 > 0$ they are not; thus the natures of the wave modes may be expected to change at or near where the solutions intersect either or both of the lines $\omega = \omega_{pr}$ and $\omega = ck_\parallel$, and $k_x^2 < 0$ for real values of $\omega$ satisfying

$$\mathrm{Min}\left(1, \frac{c^2k_\parallel^2}{\omega_{pr}^2}\right) < \frac{\omega^2}{\omega_{pr}^2} < \mathrm{Max}\left(1, \frac{c^2k_\parallel^2}{\omega_{pr}^2}\right). \tag{4.29}$$

As verified by numerical calculations, mode $A$ satisfies (4.29) until it reaches the intersection point of the lines (where $k_\parallel = \omega_{pr}/c$ and $\omega = \omega_{pr}$) and cuts off. In the short-wavelength regime, mode $B$ approaches the line $\omega = \omega_{pr}$ as $k_\parallel$ decreases, and becomes a complex-conjugate pair ($B^-$ and $B^+$) before reaching it.

## 5. Discussion

The results of Sec. 4 suggest that the thin-beam solutions fall into three categories: short-wavelength, long-wavelength and those belonging to a transition region for intermediate values of $k_\parallel$. The small-$a$ approximations can be used if $a$ is small enough that the thin-beam condition $O(|k_x^b a|) < 1$ holds. These approximations are not uniformly good (in $k_\parallel$), even for small $a$, being inaccurate near the transition re-

https://doi.org/10.1017/S002237789900793X Published online by Cambridge University Press

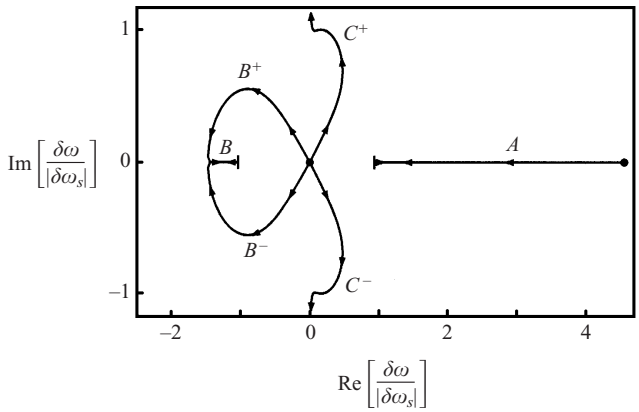


**Figure 3.** The loci of the solutions for $\delta\omega$ in the complex plane as $\alpha = ck_\parallel/\omega_p$ is varied from 0 to $2\alpha_c$ and for the same parameter values and normalization as in Fig. 1. The solutions start at a filled circle and move in the direction of the arrows as labelled, with $A$ and $B$ changing direction at the vertical lines. For even larger values of $\alpha$, mode $A$ continues beyond the right-hand side of the figure, mode $B$ beyond the left-hand side, and modes $C^+$ and $C^-$ beyond the top and bottom respectively.

gion; however, the separate transition-point solutions that we obtained are accurate for small $a$, as shown in Figs 1 and 2. The analytical study and the numerical results both imply that there are at least four distinct solutions for small $a$, outside the transition region. As $k_\parallel$ is decreased from a value in the short-wavelength regime, one real solution ($A$) cuts off at $\omega = ck_\parallel = \omega_{pr}$, whereas a second real solution (B) becomes a complex-conjugate pair ($B^+$ and $B^-$) near the transition region. Mode $B^+$ is unstable, with (4.24) giving a reasonable estimate for the maximum growth rate, which occurs for $k_\parallel \approx \omega_{pr}/U$. There are two 'radiative' modes ($C^+$ and $C^-$) for all values of $k_\parallel$. Figure 3 shows how the solutions move in the complex plane as $k_\parallel$ is varied for values of parameters consistent with the small-$a$ approximation.

Previous discussion of the beam/plasma system in planar geometry by Schmidt (1979) and by Asséo et al. (1980) did not include the thin-beam results presented here. These, however, appear to be directly related to the thin-beam results obtained by APS83 and A95 for the *cylindrical*-geometry case, as we discuss further below. They are important, since they are the only results that lead to instability, when the beam is immersed in a surrounding plasma (mode $B^+$), and in the cylindrical case appear to lead to the radiative instability of Goldreich and Keeley (1971).

It is instructive to briefly compare our results with those obtained in cylindrical geometry by APS83 and A95. In these papers, a beam of thickness $a$ and exterior radius $r_0$ of relativistic electrons and positrons was considered, flowing with angular frequency $\mathbf{\Omega}_0$ along an azimuthal magnetic field of infinite magnitude that constrains the particles to move azimuthally. The boundary conditions used (continuity of the electric and magnetic fields across the beam boundaries) were the same as applied here. Thin-beam and thick-beam cases were identified with $a/r_0 \ll \delta\omega/\omega_R$ and $a/r_0 \gg \delta\omega/\omega_R$ respectively. The component $k_x^b$ of the wavevector in the planar case has an analogue in the cylindrical case that appears in the arguments of Bessel functions, $k_r^b = \omega W_b^{1/2}/c$. Using the approximation (4.1$b$) for $W_b$, one finds that $|k_r^b a| \ll 1$ for the thin-beam case, in analogy with our definition.

For the thin-beam case, APS83 obtain (to lowest order in $a/r_0 \ll 1$) a 'radiative

https://doi.org/10.1017/S002237789900793X Published online by Cambridge University Press

instability' with growth rate

$$\omega_i \approx 0.4 \frac{\omega_p}{\gamma_p^{3/2}} m^{1/3} \left(\frac{a}{r_0}\right)^{1/2}, \tag{5.1}$$

for a beam embedded in vacuum, apparently reproducing the radiative instability of Goldreich and Keeley (1971). In the above, $m$ is the azimuthal wavenumber. It is reasonable to expect to reproduce this result from the simpler planar-geometry calculation, because $r_0 \gg a$ and the perpendicular wavelength inside the beam is much larger than the beam thickness, so that the beam is not resolved. This would imply that only the global geometry is important, and this can be represented mathematically by additional constraints on the wave fields. Our result corresponding to (5.1) is

$$|\delta\omega| = 0.7 \frac{\omega_p}{\gamma_p^2} (|k_\parallel| a)^{1/2}, \tag{5.2}$$

and, writing $k_\parallel = m/r_0$, we obtain

$$|\delta\omega| = 0.7 \frac{\omega_p}{\gamma_p^2} |m|^{1/2} \left(\frac{a}{r_0}\right)^{1/2}. \tag{5.3}$$

The $a$ dependence is the same in (5.1) and (5.3); however, the dependence on $m$ and $\gamma_p$, as well as the numerical factors in front, differ. The above arguments suggest that the differences between the results are due to the choice of the waves in the vacuum (here a single plane wave and in the cylindrical case waves with Bessel-function form), or equivalently to the choice of global geometry.

## 6. Conclusions

In conclusion, we find here that instability only occurs for the planar case if the beam is immersed in a surrounding plasma, not vacuum, and this instability occurs for mode $B^+$ as described above. These results are opposite to those of APS83 and A95 (for cylindrical geometry), who find radiative instability for a beam surrounded by vacuum, the instability being quenched in the presence of a surrounding plasma. We hope to consider the connection between the planar and cylindrical cases further in a forthcoming paper.

## Appendix. Group velocity and velocity of energy propagation

Solutions of (2.4) may formally be written in the form $\omega = \omega_M(\mathbf{k})$ or alternatively $k_x = k_{xM}(\omega, \mathbf{k}_s)$ for a given mode $M$ such that

$$\Lambda(\omega_M(\mathbf{k}), \mathbf{k}) = 0, \tag{A 1a}$$

$$\Lambda(\omega, k_{xM}(\omega, \mathbf{k}_s), \mathbf{k}_s) = 0. \tag{A 1b}$$

Differentiation of (A 1a) with respect to $\mathbf{k}$ leads to

$$\mathbf{v}_{gM}(\mathbf{k}) = \frac{d\omega_M(\mathbf{k})}{d\mathbf{k}} = -\left.\frac{\partial\Lambda(\omega, \mathbf{k})/\partial\mathbf{k}}{\partial\Lambda(\omega, \mathbf{k})/\partial\omega}\right|_{\omega_M(\mathbf{k})}, \tag{A 2}$$

where $\mathbf{v}_{gM}(\mathbf{k})$ is identified as the group velocity of the waves in mode $M$ around $\mathbf{k}$. Partial differentiation of (A 1b) with respect to $\omega$ and $\mathbf{k}_s$ then implies the alternative

https://doi.org/10.1017/S002237789900793X Published online by Cambridge University Press

forms

$$v_{gxM}(\mathbf{k}) = \left.\frac{1}{\partial k_{xM}(\omega,\mathbf{k}_s)/\partial\omega}\right|_{\omega_M(\mathbf{k})}, \tag{A 3}$$

$$\mathbf{v}_{gsM}(\mathbf{k}) = -v_{gxM}(\mathbf{k})\left.\frac{\partial k_{xM}(\omega,\mathbf{k}_s)}{\partial\mathbf{k}_s}\right|_{\omega_M(\mathbf{k})}, \tag{A 4}$$

where we use subscripts $x$ and $s$ to denote the components of $\mathbf{v}_{gM}(\mathbf{k})$ in the $x$ direction and in the $(y,z)$-plane respectively. The group velocity $\mathbf{v}_{gM}(\mathbf{k})$ is generally identified as the velocity at which the wave energy propagates; however, this assumes that the wavevector $\mathbf{k}$ is real or predominantly real (in the case of waves that are not uniformly excited over all space). When $\mathbf{k}$ is not real, as in the case of modes $C^+$ and $C^-$, which have predominantly imaginary $k_x$ in the bounding plasmas, $\mathbf{v}_{gM}(\mathbf{k})$ is imaginary or complex and cannot be identified as the velocity of energy propagation.

Consider (4.2a), which is obtained by expanding the perpendicular wavenumber $k_x^r = k_{xM}(\omega_R+\delta\omega,\mathbf{k}_s)$ to first order in $\delta\omega$, using (A 3) and (A 4), $k_{xR}^r = k_{xM}(\omega_R,\mathbf{k}_s)$ and $v_{gx}^r = v_{gxM}(k_{xR}^r,\mathbf{k}_s)$, with $\omega_M(k_{xR}^r,\mathbf{k}_s) = \omega_R$. Equation (4.2a) can be written in the form

$$\delta\omega - \delta k_x^r v_{gx}^r = 0, \tag{A 5}$$

where we define $\delta k_x^r = k_x^r - k_{xR}^r$. Multiplying (A 5) by the total wave energy $\bar{W}_M(\mathbf{k}_s)$ in mode $M$ and taking the imaginary part, we obtain

$$\omega_i(\mathbf{k}_s)\bar{W}_M(\mathbf{k}_s) - k_{xi}^r(\mathbf{k}_s)\bar{F}_{xM}(\mathbf{k}_s) = 0, \tag{A 6}$$

where $\omega_i(\mathbf{k}_s) = \mathrm{Im}[\delta\omega]$, $k_{xi}^r(\mathbf{k}_s) = \mathrm{Im}[k_x^r]$ and $\bar{F}_{xM}(\mathbf{k}_s)$ is the $x$ component of

$$\bar{\mathbf{F}}_M(\mathbf{k}_s) = \tilde{\mathbf{v}}_{gM}(\mathbf{k}_s)\bar{W}_M(\mathbf{k}_s), \tag{A 7}$$

with

$$\tilde{v}_{gxM}(\mathbf{k}_s) = \frac{\mathrm{Im}[\delta k_x^r v_{gx}^r]}{\mathrm{Im}[k_x^r]}, \tag{A 8}$$

$$\tilde{\mathbf{v}}_{gsM}(\mathbf{k}_s) = \mathbf{v}_{gsM}(k_{xR}^r,\mathbf{k}_s). \tag{A 9}$$

Equation (A 6) can be interpreted as an equation for conservation of energy in the absence of source terms,

$$\frac{\partial\bar{W}(t,\mathbf{x},\mathbf{k}_s)}{\partial t} + \boldsymbol{\nabla}\cdot\bar{\mathbf{F}}(t,\mathbf{x},\mathbf{k}_s) = 0, \tag{A 10}$$

where

$$\bar{W}(t,\mathbf{x},\mathbf{k}_s) = \bar{W}_M(\mathbf{k}_s)e^{2[\omega_i(\mathbf{k}_s)t - k_{xi}^r(\mathbf{k}_s)x]}, \tag{A 11}$$

$$\bar{\mathbf{F}}(t,\mathbf{x},\mathbf{k}_s) = \bar{\mathbf{F}}_M(\mathbf{k}_s)e^{2[\omega_i(\mathbf{k}_s)t - k_{xi}^r(\mathbf{k}_s)x]}, \tag{A 12}$$

and one thus identifies $\bar{\mathbf{F}}_M(\mathbf{k}_s)$ as the energy density flux per unit $\mathbf{k}_s$ space. It follows that the velocity of energy propagation is given by $\tilde{\mathbf{v}}_{gM}(\mathbf{k}_s)$. The above results are derived for a plasma that is non-dissipative and with $\mathbf{k}_{si} = 0$, but the identification of the energy propagation velocity remains the same if dissipative effects are included and $\mathbf{k}_{si} \neq 0$. Equation (A 6) implies that an alternative form to

https://doi.org/10.1017/S002237789900793X Published online by Cambridge University Press

(A 8) in our case is

$$\tilde{v}_{gxM}(\mathbf{k}_s) = \frac{\omega_i(\mathbf{k}_s)}{k^r_{xi}(\mathbf{k}_s)} = \frac{\mathrm{Im}[\delta\omega]}{\mathrm{Im}[k^r_x]}, \tag{A 13}$$

as in (4.12).

## References


Asséo, E. 1995 The importance of boundary effects in the emission region of the pulsar magnetosphere. *Mon. Not. R. Astron. Soc.* **276**, 74–102.

Asséo, E., Pellat, R. and Rosado, M. 1980 Pulsar radio emission from beam plasma instability. *Astrophys. J.* **239**, 661–670.

Asséo, E., Pellat, R. and Sol, H. 1983 Radiative or two-stream instability as a source for pulsar radio emission. *Astrophys. J.* **266**, 201–214.

Buschauer, R. and Benford, G. 1978 Physical mechanism of the Goldreich-Keeley radiative instability. *Mon. Not. R. Astron. Soc.* **185**, 493–506.

Buschauer, R. and Benford, G. 1979 Fundamental radiative instability of accelerated plasmas. *Phys. Fluids* **22**, 1297–1305.

Cally, P. S. 1986 Leaky and non-leaky oscillations in magnetic flux tubes. *Solar Phys.* **103**, 277–298.

Goldreich, P. and Keeley, D. A. 1971 Coherent synchrotron radiation. *Astrophys. J.* **170**, 463–477.

Rankin, J. M. 1992 An empirical theory of pulsar emission. In: *The Magnetospheric Structure and Emission Mechanisms of Radio Pulsars. Proceedings of IAU Colloquium 128* (ed. T. H. Hankins, J. M. Rankin and J. A. Gil), pp. 133–139. Pedagogical University Press, Zielona Gora, Poland.

Rowe, G. W. 1993 Collisionless damping of fast and ion-cyclotron surface waves. *Aust. J. Phys.* **46**, 271–304.

Rowe, G. W. and Rowe, E. T. 1999 Beam stability in strongly magnetized pair plasmas. Part 2. *J. Plasma Phys.* **62**, 441–448.

Schmidt, G. 1979 *Physics of High Temperature Plasmas*. Academic Press, New York.